Probing the Structure and Function of Human Glutaminase-Interacting Protein: A Possible Target for Drug Design[†,‡]

Monimoy Banerjee,[§] Chengdong Huang,[§] Javier Marquez,[||] and Smita Mohanty*[,§]

Department of Chemistry and Biochemistry, Auburn University, Auburn, Alabama 36849, and Departamento de Biología Molecular y Bioquímica, Laboratorio de Química de Proteínas, Facultad de Ciencias, Universidad de Málaga, 29071, Málaga, Spain

Received February 18, 2008; Revised Manuscript Received July 9, 2008

ABSTRACT: PDZ domains are one of the most ubiquitous protein−protein interaction modules found in living systems. Glutaminase interacting protein (GIP), also known as Tax interacting protein 1 (TIP-1), is a PDZ domain-containing protein, which plays pivotal roles in many aspects of cellular signaling, protein scaffolding and modulation of tumor growth. We report here the overexpression, efficient refolding, single-step purification, and biophysical characterization of recombinant human GIP with three different C-terminal target protein recognition sequence motifs by CD, fluorescence, and high-resolution solution NMR methods. It is clear from our NMR analysis that GIP contains 2 α-helices and 6 β-strands. The three target protein C-terminal recognition motifs employed in our interaction studies are glutaminase, β-catenin and FAS. This is the first report of GIP recognition of the cell surface protein FAS, which belongs to the tumor necrosis factor (TNF) receptor family and mediates cell apoptosis. The dissociation constant (K_D) values for the binding of GIP with different interacting partners as measured by fluorescence spectroscopy range from 1.66 to 2.64 μM. Significant chemical shift perturbations were observed upon titration of GIP with above three ligands as monitored by 2D {^{1}H,^{15}N}-HSQC NMR spectroscopy. GIP undergoes a conformational change upon ligand binding.

Cellular signaling systems are an important part of physiological function, and are mediated largely by protein−protein interactions. One of the most well-known protein−protein interaction motifs, the PDZ (postsynaptic density protein, disc large, zona occludens) domain (*1, 2*), is present in several hundred human proteins (*3*). These PDZ motifs are small interaction modules normally spanning 80−100 amino acid residues. PDZ domains mediate various signaling pathways (*4*), localize and cluster ion-channels and membrane receptors, maintain cell polarities (*5*), and are involved in scaffolding of multimeric complexes by recognizing the C-terminal amino acid sequence motif of the interacting proteins (*6, 7*). These interactions localize membrane proteins to specific subcellular domains, enabling the assembly of supramolecular complexes. Many of these proteins possess several PDZ domains within the same protein, or are associated in multimeric complexes which form a conglomeration of PDZ modules.

Human glutaminase-interacting protein (GIP) is a small soluble multifunctional protein containing one PDZ domain. GIP was originally identified in a yeast two-hybrid genetic selection system while looking for interactors of glutaminase in human brain (*8*). GIP interacts with the C-terminus of glutaminase L (liver type), which is responsible for synaptic transmission and regulation of cerebral concentrations of glutamine and neurotransmitter glutamate (*8*). Apart from the fact that glutaminase is crucial for the normal activity of the central nervous system, this enzyme also plays a key role in tumor development (*9*). Glutamine is an essential nutrient for tumor tissues, and glutamine-related anticancer therapy involves clearance of circulatory glutamine by glutaminase. A partial GIP cDNA clone was previously identified from human lymphocytes through a yeast two-hybrid screening and named TIP-1, for Tax-interacting protein 1, because it is a binding partner for the viral oncoprotein Tax (*10*).

The full-length human GIP cDNA encodes a 124-residue protein. This protein contains a single PDZ domain encompassed by residues 17−112 of the protein sequence (*8*). While the exact mechanism by which GIP and glutaminase interact in the brain is not yet elucidated, colocalization of both proteins in astrocytes and neurons suggest the role of GIP as an important scaffolding PDZ protein in the mammalian brain (*11*). GIP may contribute to the determination of the subcellular distribution and localization of glutaminase and/or regulation of its function (*11, 12*). Apart from glutaminase, a plethora of binding partners have been reported, implicating GIP in key biological processes. The

[†] This research was financially supported by USDA PECASE Award 2003-35302-12930 (Presidential Early Career Award for Scientists and Engineers to S.M.) and NSF Grant IBN-0628064 (to S.M.) and SAF2004-02339 Grant (to J.M.) from the Ministry of Education and Science of Spain.

[‡] Author contributions: S.M. designed research; S.M., M.B. and C.H. performed research and collected all data; S.M., M.B. and C.H. analyzed data; J.M. provided original clone, GST-glutaminase bound resin and anti-GIP antibodies; S.M., M.B. and C.H. prepared the manuscript.

* Corresponding author. Phone: +1 334-844-7081. Fax: +1 334-844-6569. E-mail: mohansm@auburn.edu.

[§] Auburn University.

[||] Universidad de Málaga.

10.1021/bi800287v CCC: $40.75
Published on Web 08/09/2008

other reported GIP binding partners are the viral oncoproteins HTLV-1 Tax (*10*), HPV16 E6 (*13*), and the Rho-activator rhotekin (*14*), which involves GIP in the Rho signaling pathway, and the potassium channel Kir 2.3, where GIP regulates channel expression in the plasma membrane of renal epithelia (*15*). GIP has also been shown to participate in the regulation of transcription; it binds to the C-terminus of β-catenin (*16*−*18*). β-catenin mediates Wnt signaling involved in regulation of cell−cell adhesion during embryogenesis; however, deregulation of the signal transduction pathway frequently leads to the formation of various cancerous tumors (*16*−*18*). Overexpression of GIP reduces the proliferation and anchorage-independent growth of colorectal cancer cells (*16*).

GIP is not only involved in the CNS (central nervous system) and various human cancers; we discovered that it also interacts with the C-terminal region of a cell-surface protein FAS, which belongs to the TNF (tumor necrosis factor) receptor family (*19*) and mediates cell apoptosis (*20, 21*).

GIP belongs to class I PDZ domain, which recognizes the C-terminal sequence (S/T)-X-Φ of the peptides (X denoting any amino acid and Φ representing a hydrophobic residue). The residues at positions 0 and −2 of the peptide (position 0 referring to the C-terminal residue) play a critical role in the specificity and affinity of the interaction (*16*). Class I PDZ domains usually contain 6β (β1−β6) strands and 2α (α1−α2) helices. It has been reported that the PDZ domain binds the C-terminus of the interaction partner in an elongated groove as an antiparallel β-strand between the second α-helix and the second β-strand, termed the PDZ binding groove (*22*). The well-conserved Gly-Leu-Gly-Phe (GLGF) motif, known as the carboxylate-binding loop, is located within the β1−β2 connecting loop and is important for hydrogen bond coordination of the C-terminal carboxylate group (COO^-) (*3*).

Because PDZ proteins have well-defined binding sites, they are promising targets for drug discovery. Furthermore, GIP is one of the smallest members of the PDZ family, containing only one PDZ domain that represents its full primary structure, thus offering itself as a very suitable candidate for structural studies. Structure, function, and interaction studies of GIP with the C-terminal recognition motif of different binding partners will provide us the insight into the mechanisms of action of this multifunctional protein, which is indeed a necessary prelude for successful drug design. We report here an efficient method for production of pure recombinant GIP, structural characterization by CD, fluorescence and high-resolution solution NMR, and interaction studies with 3 different binding partners. A mechanism of the interactions of GIP with the partner protein recognition motifs has been proposed.

EXPERIMENTAL PROCEDURES

Cloning and Overexpression of GIP. The 1.3-kb cDNA encoding GIP was originally cloned into the pJG4-5 vector (*23*). This construct was used as template DNA for PCR. To express only the 13.7 kDa GIP protein without any additional residues, the open reading frame (ORF) sequence was amplified and cloned into the *Nde*I/*Bam*HI (Invitrogen) sites of the pET-3c vector (Novagen), using the following primers: forward, 5′-AGC-AGG-GTC-CAT-ATG-TCC-TAC-ATC-CCG-3′, and reverse, 5′-CGG-CAG-GCA-GGA-TCC-GCA-GAT-GGT-GG-3′. The recombinant pET-3c/GIP plasmid was transformed into *Escherichia coli* BL21 DE3pLys cells, and expression was performed. Saturated LB-ampicillin starter culture was diluted (1:25, v/v) in LB media and grown at 37 °C to an A_{600} of 0.55. Expression was induced with 1 mM IPTG, and cells were harvested by centrifugation after incubation for 4 h. Reducing the incubation temperature to 30 °C increased the soluble protein to some extent. The bacterial cells, suspended in 50 mM phosphate buffer at pH 8 containing 200 mM NaCl, 4 mM EDTA, 4% glycerol, and 1 mM PMSF, were lysed by sonication. After centrifugation, both supernatant and pellet-containing GIP inclusion bodies (IBs) were collected. IBs were refolded as described below. For production of ^{15}N- and ^{15}N,^{13}C-labeled proteins, bacterial cells were grown in minimal media containing ^{15}N-labeled ammonium chloride and either regular or ^{13}C-labeled glucose.

Refolding of Chemically Denatured GIP Inclusion Bodies. Approximately 6.5 mg of GIP IBs were weighed out in a microfuge tube and washed with 10% B-PER (bacterial protein extraction reagent, Pierce Biotechnology) solution twice. The IBs were solubilized with 6 M guanidine hydrochloride solution to a total volume of 1 mL and left overnight at room temperature. Insoluble particles were removed by centrifugation. Renaturation of GIP was initiated by dilution with refolding buffer in the presence of 10% α-cyclodextrin or 400 mM L-arginine or without any additive (control experiment) at room temperature (Table S1 in Supporting Information). The final concentration of guanidine hydrochloride was 285 mM. The refolded protein was subjected to purification as described below.

Purification of GIP. Both the soluble and refolded GIP were purified in a single step by size exclusion chromatography with a Sephacryl S-100 column (GE Healthcare) fitted to an FPLC system using 20 mM phosphate buffer of pH 6.5, 150 mM NaCl, 1 mM EDTA and 0.1% NaN_3 as the mobile phase.

Western Blotting and In Vitro Pull-down Assay. Western blotting was carried out on both soluble and refolded GIP following the procedures reported earlier (*8, 23*).

Fluorescence. All fluorescence spectra were recorded on a PerkinElmer Precisely LS 55 Luminescence spectrofluorometer at 25 °C (λ_{ex} 295 nm for acrylamide and 280 nm for iodide and ligands). Emission spectra were recorded over the range 300−500 nm with 1 nm steps. All experiments were carried out in 20 mM phosphate buffer, pH 6.5, 150 mM NaCl, 0.1 mM EDTA and 0.01% NaN_3. Stock solutions of the quenchers were prepared in water at 5 M concentration. Aliquots of these solutions were directly added to a cuvette containing 2 mL of 1−4 μM GIP. All titration experiments were corrected to take into account the dilution effect. Emission from the controls were corrected by recording subtraction spectra between sample and control probes.

Circular Dichroism (CD). All circular dichroism (CD) experiments were performed on a Jasco J-810 automatic recording spectropolarimeter. Both far-UV and near-UV CD spectra were measured in a 0.05 cm quartz cell at room temperature. The buffer used was 20 mM phosphate buffer (pH 6.5). The protein concentration was 10−20 μM. Data were averaged over 100 scans for each protein sample and over 50 scans for each control sample. Response time was

1 s, and scan speed was 100 nm min^{-1}. For tertiary structure determination, 800 μM GIP was used.

Nuclear Magnetic Resonance (NMR). All NMR data were collected at 298 K on a Bruker Avance 600 MHz spectrometer equipped with triple resonance H/C/N TCI cryoprobe at the Department of Chemistry and Biochemistry, Auburn University, processed using NMRPipe (*24*), and analyzed using NMRView (*25*). The sample contained ~800 μM uniformly $^{15}N/^{13}C$ labeled GIP, 50 mM phosphate buffer containing 5% D_2O (pH 6.5), 1 mM EDTA and 0.01% (w/v) NaN_3. The following spectra were used for the sequential assignment of ^1H_N, $^1H_\alpha$, ^{15}N, $^{13}C_\alpha$, $^{13}C_\beta$ and ^{13}CO resonances: 2D {^1H,^{15}N}-HSQC, 3D HNCACB, 3D CC(CO)NH, 3D CBCACONH, 3D ^{15}N edited HSQC-TOCSY with a mixing time of 80 ms, 3D ^{15}N edited HSQC-NOESY with a mixing time of 200 ms, 3D HCCONH, 3D HNHA, 3D HNCO and 3D HNCACO. $^1H_\alpha$, $^{13}C_\alpha$, $^{13}C_\beta$ and ^{13}CO chemical shifts were used to determine the secondary structure using the programs PSSI (*26*) and PsiCSI (*27, 28*). Ligand titration experiments were performed and monitored by a series of two-dimensional ^{15}N-edited HSQC experiments.

Interaction studies were carried out by titration of 100 μM GIP with three different C-terminal target sequences: the C-terminus of glutaminase (KENLESMV-COOH), β-catenin (FDTDL-COOH), (FDTDL-$CONH_2$) and FAS (NEIQSLV-COOH). The amide chemical shift perturbations ($\Delta\delta$) were calculated as $\Delta\delta = |\Delta\delta^{15}N|/f + |\Delta\delta^{1}H|$ (*29, 30*). The introduction of the *f* factor and its value were justified by the difference in the spectral widths of the backbone ^{15}N resonances and the ^1H signals (^{15}N range, 131.8−100.4 ppm = 31.4 ppm; ^1H range, 10.1−6.5 ppm = 3.6; correction factor $f = 31.4/3.6 = 8.7$). Thus, the correction factor $f =$ 8.7 was used in order to give roughly equal weighting for each of the ^1H and ^{15}N chemical shift changes. ModelTitr program (*31*) was used to calculate dissociation constant values of various residues of GIP. The target peptides were obtained with >95% purity from Genemed Synthesis (CA), Synbiosci (CA) or Chi Scientific (MA). The 5−20 mM stock solutions of the above peptides were prepared in 10 mM phosphate buffer at pH 6.5 for NMR, CD and fluorescence titration experiments.

RESULTS

Protein Expression Optimization. The GIP gene was cloned into the pET-3c vector. Protein expression was optimized using three different *E. coli* strains, different temperatures and different IPTG concentrations. BL21DE3-pLys was found to be the best host for the expression of GIP. GIP was produced primarily in IBs when expressed in LB media (or minimal media) at 37 °C for 4 h (12 h for minimal media) after induction with 1 mM IPTG. About 95% of GIP was expressed in IBs at 37 °C in BL21DE3pLys cells. The expression of soluble GIP was increased to some extent by reducing the temperature to 30 °C. ^{15}N-labeled and ^{15}N,^{13}C-labeled GIP were expressed in *E. coli* cells grown in minimal media containing ^{15}N-labeled ammonium chloride and either regular or ^{13}C-labeled glucose.

Refolding of Inclusion Bodies (IB). To optimize refolding, 8 different buffer conditions were used in the presence or absence of additives (α-cyclodextrin or L-arginine) over a pH range of 5.0 to 10.0 (Table S1 in Supporting Information). The refolding data indicated that Tris-HCl buffer at pH 8.0

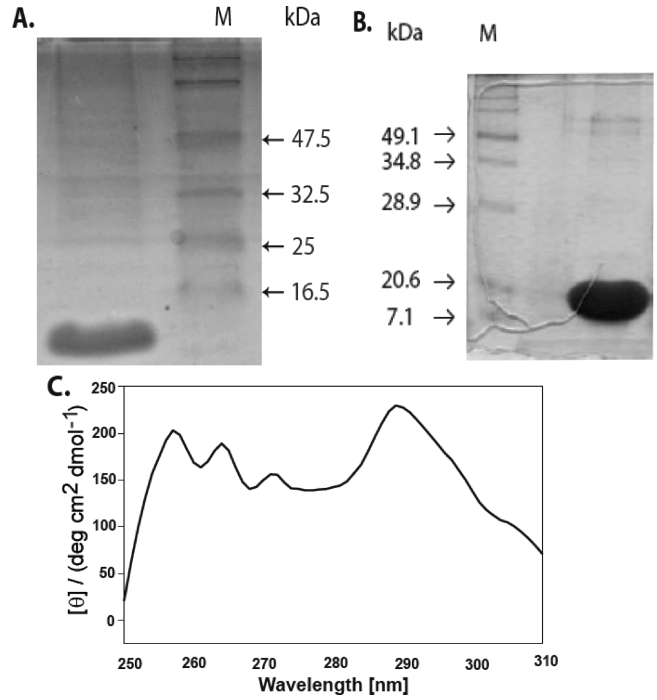

FIGURE 1: 15% SDS−PAGE gel: (A) SDS−PAGE analysis of pure {^{13}C,^{15}N} soluble GIP after size exclusion chromatography. The lanes are protein marker (M) and soluble GIP. (B) SDS−PAGE analysis of pure refolded GIP after size exclusion chromatography. The lanes are protein marker (M) and refolded GIP. (C) Near-UV CD spectrum of GIP in phosphate buffer (pH 6.5) at 25 °C.

produced the highest yield of active GIP in the absence of any additive. However, the yield increased by 5.6% with the addition of 10% α-cyclodextrin and by 1.9% in the presence of 400 mM L-arginine (Table S1 in Supporting Information).

Protein Purification. Protein purification was optimized by trying various methods. However, both soluble (Figure 1A) and refolded GIP (Figure 1B) were purified to homogeneity in a single step by size-exclusion chromatography on a Sephacryl S-100 column (GE Healthcare).

Recombinant GIP was successfully isotope-enriched (both ^{15}N and ^{15}N,^{13}C) and purified to homogeneity with the above protocol. About 56 mg of pure uniformly labeled GIP (^{15}N or ^{15}N,^{13}C) was obtained per liter of bacterial culture.

Characterization and Interaction Studies of GIP. (a) In Vitro Pull-down Assays. Protein activity of both soluble and refolded recombinant GIP was confirmed in a pull-down assay against recombinant GST-glutaminase, as described previously (*8, 23*). Pulled-down GIP was revealed by a Western blot using polyclonal anti-GIP antibodies from rabbit. A clear band of GIP was revealed, confirming the functionality of both soluble and refolded recombinant GIP (data not shown).

(b) Characterization of GIP Using Circular Dichorism (CD) and NMR Spectroscopy. The secondary structure of GIP and the effect of different buffer conditions and pH on GIP structure were characterized by far-UV CD spectroscopy, which revealed that GIP is more structured in phosphate buffer at pH 6.2. Deconvolution of CD data shows that GIP contains 8.5% α-helix and 35.5% β-strand in phosphate buffer at pH 6.2. Near-UV CD data indicated that recombinant GIP has tertiary structure, an indication of properly folded protein (Figure 1C). The well-dispersed

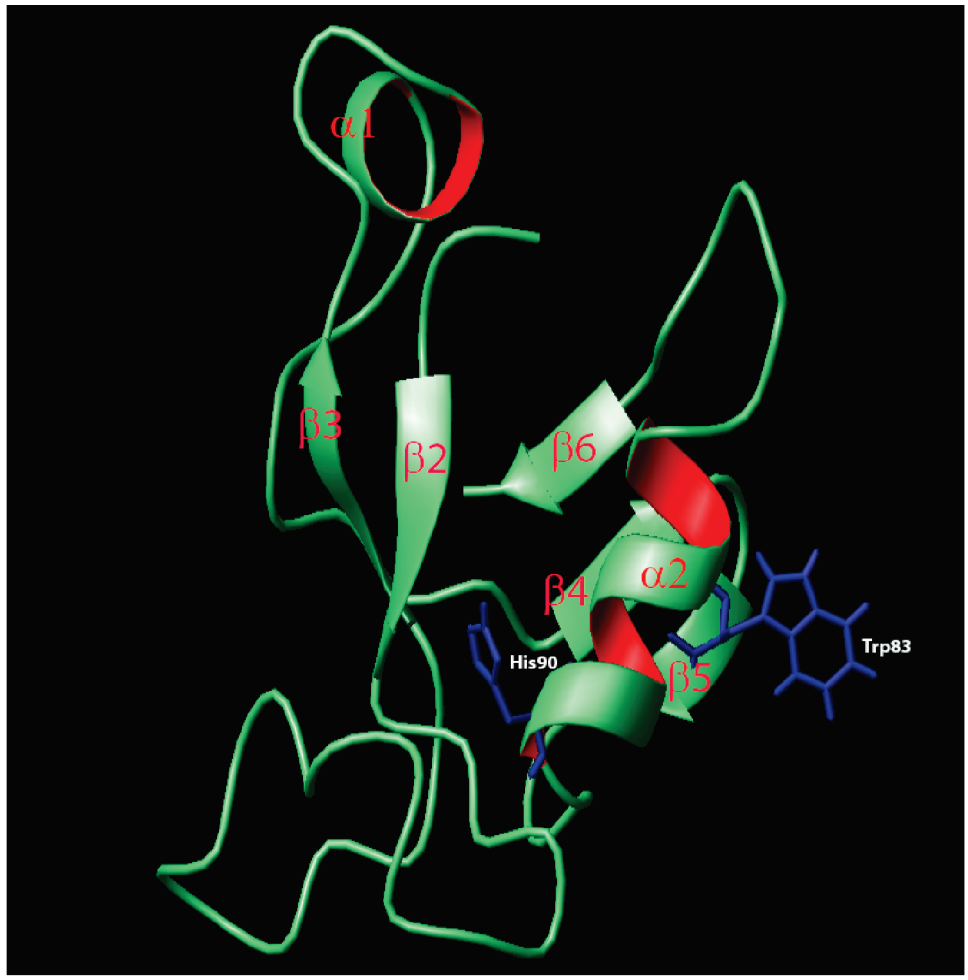

FIGURE 2: Homology based 3D model structure of GIP. Secondary structure elements are indicated. The side chain of the tryptophan residue, Trp83, and histidine residue, His90, are shown in blue and labeled. The figure was prepared with the program MOLMOL.

resonances in 2D {^{1}H,^{15}N}-HSQC spectrum in phosphate buffer also indicated that the recombinant proteins are well folded.

(c) Effect of Acrylamide and Iodide on GIP Fluorescence Emission. Tryptophan fluorescence of GIP was quenched effectively by iodide and acrylamide. For each sample, the emission maximum was observed at a wavelength of 353 nm (characteristic of solvent-exposed tryptophan) and did not shift during titration. The Stern−Volmer equation (eq 1) was used to estimate the quenching constants. The Stern−Volmer plots are approximately linear with quenching constants K_{sv}(KI) = 5.7, K_{sv}(acrylamide) = 14.4 for refolded GIP and K_{sv}(KI) = 5.6, K_{sv}(acrylamide) = 14.5 for soluble GIP.

$$I_o/I = 1 + K_{sv}[Q] \quad (1)$$

These results are consistent with the homology based model structure of GIP, in which the side chain of Trp83 is fully exposed to the solvent (Figure 2).

(d) Interactions of Target Protein Recognition Sequence Motifs and GIP by Fluorescence Spectroscopy. Addition of target peptides to GIP resulted in a small but consistent decrease in fluorescence intensity (Figure S1 in Supporting Information). The dissociation constant K_D ($K_D = 1/K_a$) was determined using the eq 2 (*32*):

$$\log [C]_f = -\log [K_a] + \log[(F_0 - F_c)/(F_c - F_i)] \quad (2)$$

From the ordinate intercept of the double reciprocal plot of $F_0/(F_0 - F_c)$ versus 1/[C], where F_0 and F_c are the fluorescence intensities of the free protein and of the protein at a peptide concentration [C], F_i, the fluorescence intensity upon saturation of all the ligand binding sites, was obtained. Assuming 1:1 ligand binding to protein, double logarithmic plots were drawn. In the plot of log $[(F_0 - F_c)/(F_c - F_i)]$ versus log [C], the abscissa intercept yielded the K_D value (the dissociation constant) for the protein−ligand interactions, which is the reciprocal of K_a (the association constant).

The titration of C-terminal peptide sequence motifs of glutaminase (KENLESMV-COOH), β-catenin (FDTDL-COOH) and FAS (NEIQSLV-COOH) with GIP resulted in a reduction in fluorescence intensity and yielded a dissociation constant of 1.66 μM, 1.94 μM and 2.64 μM respectively (Figure S1 in Supporting Information). The free energy changes of the association were calculated by using eq 3,

$$\Delta G = -RT \ln K_a \quad (3)$$

where K_a is the association constant, T is temperature and R is universal gas constant.

The corresponding ΔG values for binding of glutaminase, β-catenin and FAS C-terminus to GIP are −32.97 kJ mol^{-1}, −32.58 kJ mol^{-1}, and −31.82 kJ mol^{-1} respectively, which indicate the spontaneous nature of these bindings.

(e) Effect of Ligand Binding on GIP by CD. The effect of ligand binding on GIP secondary structure was also inves-

tigated by CD spectroscopy. As most of the PDZ domain-containing proteins require five to eight C-terminal residues for ligand binding and specificity, GIP was titrated with the peptides composed of the last 8 C-terminus residues of the ligand glutaminase (KENLESMV-COOH), the last 5 residues of the ligand β-catenin (FDTDL-COOH), and the last 7 residues of the ligand FAS (NEIQSLV-COOH).

All these peptides have very negligible contribution to the CD spectra, which is almost equivalent to the phosphate buffer. The titration of GIP with all three peptides causes significant secondary structure changes in the CD spectra of GIP (Figures S2-A, B and C in Supporting Information). However, unlike the glutaminase C-terminal protein recognition sequence motif, a small amount of white precipitation formed during the titration of β-catenin and FAS C-terminal protein recognition sequence motifs with GIP. Deconvolution of the CD data of GIP−ligand complexes was performed and the secondary structure content was calculated using the program CDPro (*33*). The deconvolution results indicate that, for all three ligands, the percentage of helix and random coil structure content decreases with increasing concentration of ligand while the percentage of β-sheet content increases. Overall for the three complexes, the helix content is reduced by 30−60%, random coil content is reduced by 5−10% and the β-sheet structure content is increased by 18−27%.

(f) Interaction of GIP with C-Terminal Target Protein Sequence Motifs by {^{1}H,^{15}N}-HSQC NMR. NMR is a very useful technique for monitoring structure−activity relationships (SAR) in studies of protein−protein or protein−ligand interactions (*34*). In the 2D {^{1}H,^{15}N}-HSQC spectra, the chemical shifts of residue/s involved in ligand binding do change. This region is extremely sensitive; any perturbation in the chemical shifts or resonances from the original positions is indicative of the change in the conformation of the protein. This change can be local, involving a few residues, or it may be an overall conformational change involving most of the residues in the protein. To investigate the binding and possible conformational change in GIP, titration studies were carried out with the three C-terminal peptide targets while monitoring the fingerprint region of the protein in the 2D {^{1}H,^{15}N}-HSQC spectra. NMR titration studies were performed for GIP with excess ($\geq$70 times) ligand. Analysis of the HSQC spectra of the titration studies indicate that significant changes in the chemical shift positions occur for the complex/es. Overlays of the HSQC spectra collected in the absence and presence of different concentrations of target peptides are shown in Figures 3, 4 and 5. The chemical shift positions of most residues of free GIP were perturbed in the HSQC spectra upon binding to C-terminal target protein recognition sequence motifs. Dissociation constant (K_D) values for various residues of GIP were calculated assuming binding stoichiometry 1:1 (Table S2 in Supporting Information). Estimates for dissociation constants (K_D), measured using fluorescence and NMR techniques, have ranged from low micromolar to mid micromolar indicating moderate affinities. It should be noted here that, depending upon techniques used, and the initial protein concentration required for a particular technique, dissociation constant does vary (*35*−*37*).

We observed that the free FAS peptide precipitated out from the buffer slowly with time. Some precipitation was observed during the CD and HSQC titration experiments of both β-catenin and FAS peptides with GIP, although the signal-to-noise ratio (S/N) of the protein was not significantly affected. However, we did not find any precipitation (by visual inspection) during titration studies carried out by fluorescence measurements. Unlike the FAS C-terminal peptide, β-catenin C-terminal peptide was stable in aqueous buffer solution, although freshly prepared ligand was always used for all titration studies. It is important to mention here that C-terminal amidated β-catenin peptide (FDTDL-$CONH_2$) does not interact with GIP (data not shown) while the unprotected C-terminal peptide (FDTDL-COOH) does bind to GIP.

(g) Chemical Shift Perturbation of GIP upon Binding to Glutaminase, β-Catenin and FAS C-Termini. Chemical shift mapping is a powerful method to investigate possible protein−ligand interactions by NMR. To investigate GIP−ligand binding, we studied the interaction of GIP with C-terminal sequence motifs of target proteins by NMR. In the {^{1}H,^{15}N}-HSQC spectra, the amide proton and nitrogen resonances of most residues shifted gradually with increasing ligand concentration, indicating that the complexes were in fast exchange on the NMR time scale except for few residues which were found to be in intermediate exchange. Glutaminase C-terminal motif caused pronounced chemical shift changes in the {^{1}H,^{15}N}-HSQC spectrum of GIP. Residues with large chemical shift changes (greater than 0.1 ppm) of their backbone amide signals were found to cluster in several regions of the GIP sequence while interacting with glutaminase C-terminus, in particular, Gln17−Arg22, Ile37−Gln39, Ser42−Gln43, Val80−Asn81, Thr98−Glu102, Val104−Arg106 and Tyr56 (Figure S3-A in Supporting Information). However, residues Gly34, Gln39, Ile55, Tyr56, Glu62, Met78 and Met87 showed chemical shift changes greater than 0.2 ppm (highly shifted amide groups). The resonances of several residues particularly Ile28, Leu29, Gly30, Ile33 and Gly35 located in the β2 strand showed severe broadening, indicating the presence of conformational exchange phenomena. The largest chemical shift changes also occurred in the long stretch Ile28−Gln39, which corresponds to the β2 strand. Analysis of the chemical shift differences between the GIP and the GIP−β-catenin complex revealed that the largest changes in the amide resonance frequencies occur for Arg106 and the residues in the polypeptide segments Ile28−Gln39, Ile55−Gly76 and Thr86−Arg96 which correspond to β2, β3, α1, β5, α2 (Figure S3-B in Supporting Information). Residues Leu29 and Gly30 also show conformational exchange. The chemical shift perturbation map of the GIP−FAS complex indicated that many residues are affected from different regions of the protein. The chemical shift difference between the GIP and GIP−FAS complex revealed that the largest changes in the amide resonance frequencies occur for Glu17−Gln23, Phe31−Gln39, Glu48−Thr58, Ser61−Glu62, Glu67, Ala69, Arg94−Glu102, Val105−Arg106, Arg111, and Lys116 (Figure S3-C in Supporting Information). Residues Gly30, Ile28, and Leu29 show conformational exchange. These results indicate that the protein undergoes a conformational change upon binding to ligands.

(h) Sequential Assignment. Assignment of ^1H_N, $^1H_\alpha$, ^{15}N, $^{13}C_\alpha$, $^{13}C_\beta$ and ^{13}CO backbone resonances was carried out

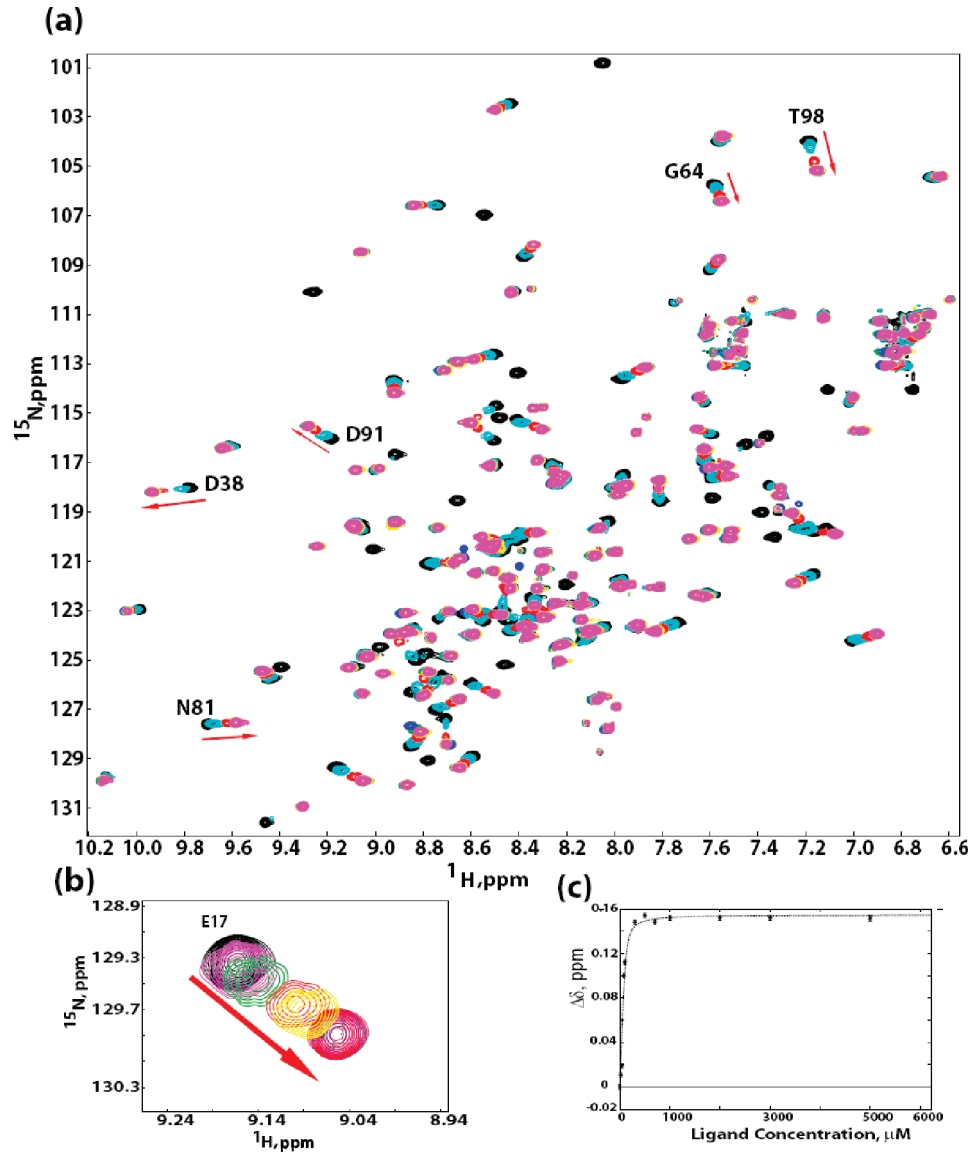

FIGURE 3: Changes of 2D {^{1}H,^{15}N}-HSQC spectrum upon addition of glutaminase (KENLESMV) to 100 μM GIP. (a) The 2D {^{1}H, ^{15}N}-HSQC spectrum demonstrating chemical shift perturbations of residues upon titration of glutaminase (KENLESMV) to GIP. Ratios of GIP to glutaminase ranges from 1:0 to 1:70. (b) Expanded regions of the spectrum demonstrating chemical shift perturbations of residue E17 upon titration of GIP with glutaminase (KENLESMV). Ratios of GIP to glutaminase are 1:0 (black), 1:0.2 (magenta), 1:0.4 (green), 1:0.8 (red), 1:1 (yellow), 1:50 (blue), 1:70 (red). (c) NMR titration curve for the titration of GIP with glutaminase (KENLESMV). The plot shows the changes in the chemical shift of D38 induced by the addition of glutaminase (KENLESMV), versus the peptide concentration. Dashed line is the titration curve as fitted by the program modelTitr from NMRPipe. The apparent dissociation constant K_D corresponding to residue D38 was determined by fitting the chemical shift change of the residue. The determined K_D value is 14.5 $\pm$ 2.3 μM.

based upon three-dimensional heteronuclear triple resonance experiments that used one- and two-bond scalar couplings to connect the atoms. 3D ^{15}N-edited HSQC-NOESY, however is based upon dipolar coupling (*38*). The 2D {^{1}H,^{15}N}-HSQC spectrum with single-letter amino acid code with residue number is shown (Figure 6). Out of 119 non-proline residues, backbone resonance assignment was completed for all residues except Met1 and Leu108, for which only the $^{13}C_\alpha$, $^{13}C_\beta$ and ^{13}CO resonances were assigned from cross peaks with their adjacent residues, Ser2 and Val109 respectively. $^{13}C_\beta$ and ^{13}CO resonances were not assigned for Leu107, as both Leu107 and Leu108 signals were very weak. $^{1}H_\alpha$ and $^{13}C_\beta$ resonances were not assigned for Leu29 and Leu71, respectively, as no peaks were detectable. $^{1}H_\alpha$, $^{13}C_\alpha$, $^{13}C_\beta$ and ^{13}CO resonances for all five proline residues were detected from their interactions with their adjacent residues. Local conformational heterogeneity complicated the assignments of the N-terminal segment. Gly6 and Ile4 show multiple peaks in the 2D {^{1}H,^{15}N}-HSQC. Gly6 showed two peaks in the 2D {^{1}H,^{15}N}-HSQC; however it is adjacent to Pro5, and the peak doubling could be due to the *cis*−*trans* conformation of Pro5. From the ratio of the intensities of the two Gly6 cross peaks, it appears that the Pro5 *cis*−*trans* conformations are present in a ratio of 1:10 at pH 6.5 and 298 K. It should be noted that this conformational change from residues 4−6 occurs on the second time scale due to the appearance of two distinct Gly6 peaks. Normally proline residues in proteins tend to be in the *trans*-conformation 95% of the time, and 5% of the time in the *cis*-conformation.

(i) Secondary Structure. The secondary structure was calculated on the basis of $^{1}H_N$, $^{1}H_\alpha$, ^{15}N, $^{13}C_\alpha$, $^{13}C_\beta$ and ^{13}CO chemical shifts using the program PSSI, which also corrected the inconsistencies in ^{13}C and ^{15}N chemical shift references. The assigned chemical shifts were referenced according to

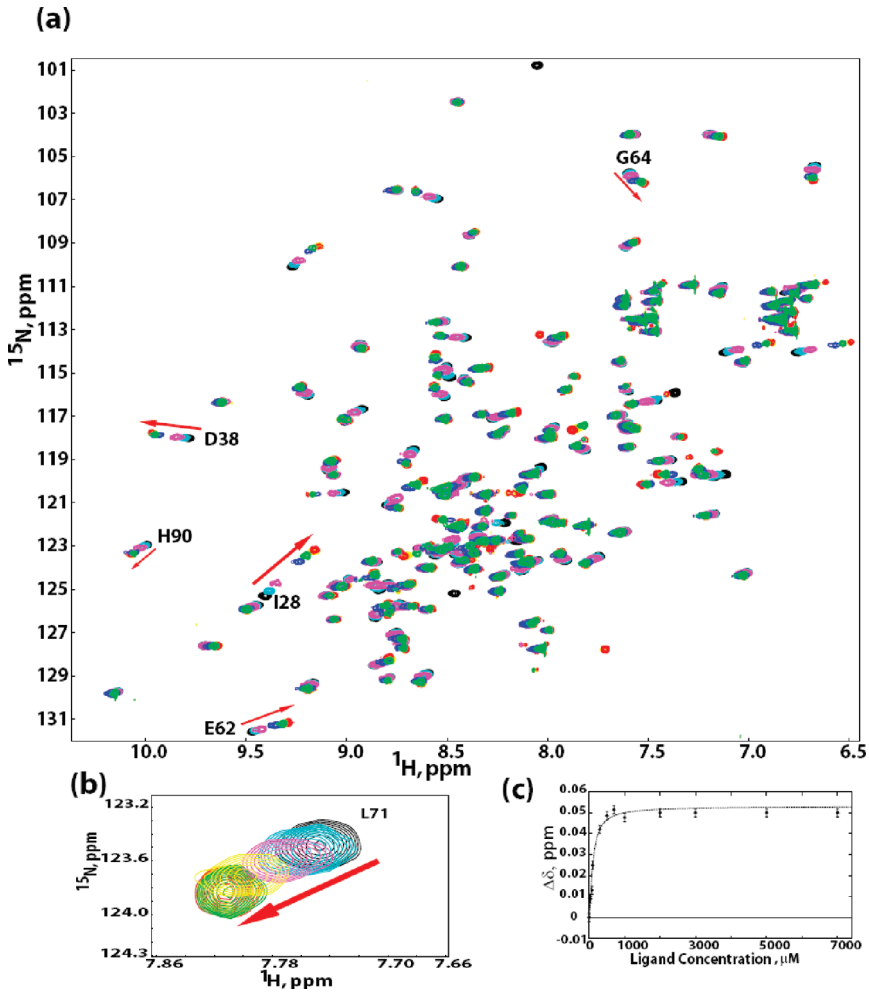

FIGURE 4: Changes of 2D {^{1}H,^{15}N}-HSQC spectrum upon addition of β-catenin (FDTDL-COOH) to 100 μM GIP. (a) The 2D {^{1}H,^{15}N}-HSQC spectrum demonstrating chemical shift perturbations of residues upon titration of β-catenin (FDTDLCOOH) to 100 μM GIP. Ratios of GIP to β-catenin (FDTDL) range from 1:0 to 1:90. (b) Expanded regions of the spectrum demonstrating chemical shift perturbations of residue L71 upon titration of GIP with β-catenin (FDTDL). Ratios of GIP to β-catenin (FDTDL) are 1:0 (black), 1:0.4 (cyan), 1:1 (magenta), 1:20 (yellow), 1:70 (red), 1:90 (green). (c) NMR titration curve for the titration of GIP with β-catenin. The plot shows the changes in the chemical shift of L71 induced by the addition of β-catenin, versus the peptide concentration. Dashed line is the titration curve as fitted by the program modelTitr from NMRPipe. The apparent dissociation constant K_D, corresponding to residue L71, was determined by fitting the chemical shift change of the residue. The determined K_D value is 21.6 $\pm$ 3.5 μM.

the PSSI results and exported to the PsiCSI program for the secondary structure calculation. These results indicate that at pH 6.5 and 298 K GIP consists of six β-strands and two α-helices with residues: 11−23 (β1), 27−35 (β2), 54−60 (β3), 64−70 (α1), 76−81 (β4), 83−88 (β5), 90−100 (α2) and 103−112 (β6) (Figure 7).

(j) Molecular Model and Refinement. A molecular model was constructed for the residues ranging from Leu29 to Leu108 using the coordinates of the second PDZ domain of human scribble protein (PDB code 1whaA), which is similar but nonidentical to GIP. Human scribble protein shares 43% sequence identity with GIP. The rough model was constructed with SWISS-MODEL (*39, 40*), solvated and subjected to constraint energy minimization with the program GROMACS (*41*). The three-dimensional visualization was performed on a UNIX workstation using the MOLMOL program (*42*).

DISCUSSION

Because GIP plays a pivotal role in many cellular signaling pathways, it is considered an excellent drug target (*43*). For successful drug design, understanding the mechanisms of protein−protein interactions, binding, recognition and specificity are very critical.

Recombinant GIP has been produced in minimal media with a yield of 56 mg/L for structural, functional and protein−protein interaction studies. Cyclodextrin was found to be a good additive for refolding of recombinant proteins. The yield of functionally refolded GIP was increased by >5% when refolding of IBs was carried out with cyclodextrin. The single tryptophan residue present in the GIP protein is a convenient feature for fluorescence studies. Tryptophan acts as an ideal intrinsic fluorescence probe, as it has the largest molar absorption coefficient, and its fluorescence intensity (I_F) and wavelength of maximum intensity (λ_{max}) are sensitive to the microenvironment of the indole group (*44*). The λ_{max} of the tryptophan residue of GIP was red-shifted to 353 nm, characteristic of a solvent-exposed tryptophan side chain. The tryptophan side chain is highly accessible to both acrylamide and potassium iodide (*45, 46*) quenchers. The K_{sv} value for acrylamide corresponds closely with that of solvent-exposed tryptophan; the K_{sv} values

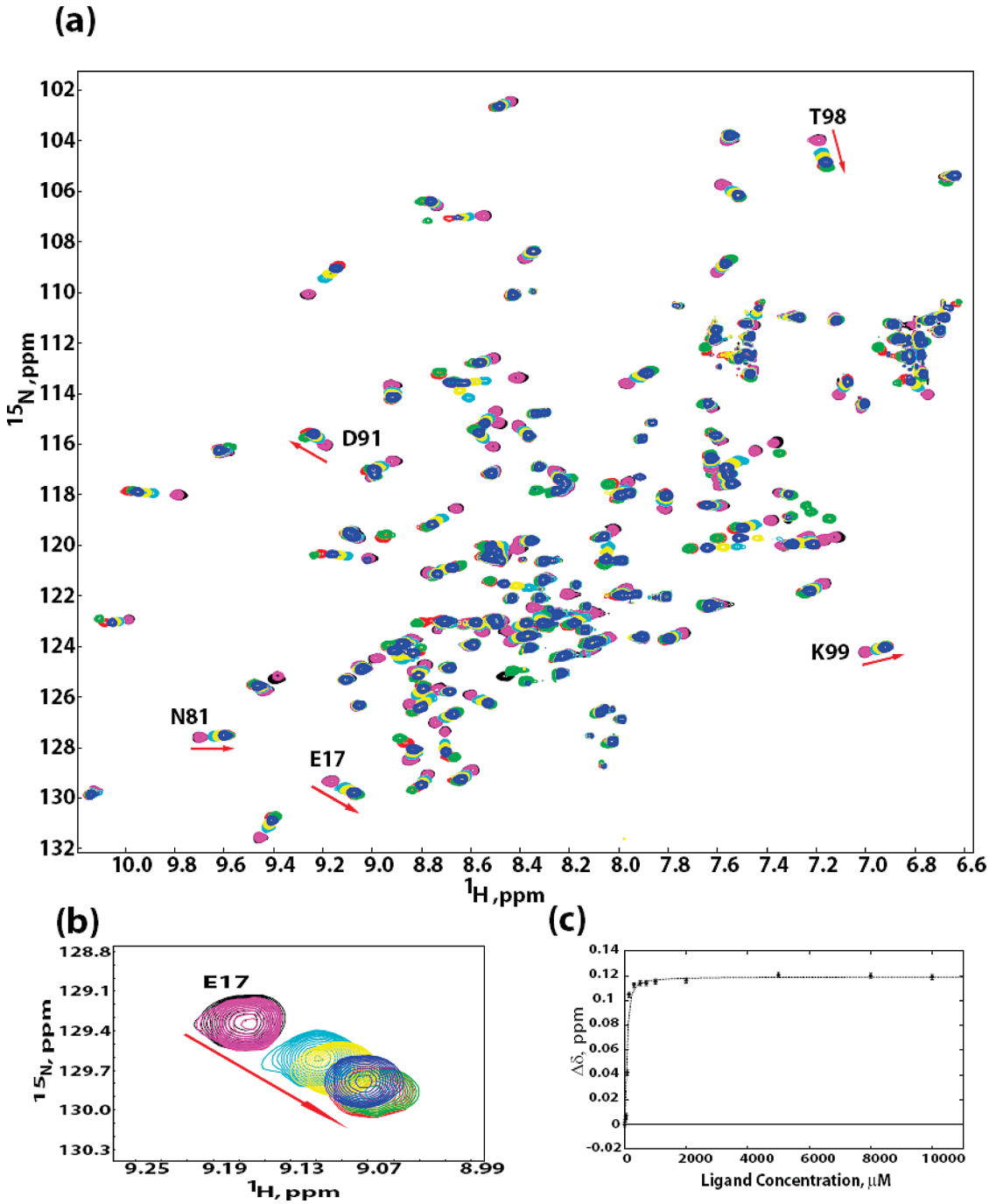

FIGURE 5: Changes of 2D {^{1}H,^{15}N}-HSQC spectrum upon addition of FAS (NEIQSLV) to 100 μM GIP. (a) The 2D {^{1}H,^{15}N}-HSQC spectrum demonstrating chemical shift perturbations of residues upon titration of FAS (NEIQSLV) to GIP. Ratios of GIP to FAS (NEIQSLV) range from 1:0 to 1:100. (b) Expanded regions of the spectrum demonstrating chemical shift perturbations of residue E17 upon titration of GIP with FAS (NEIQSLV). Ratios of GIP to FAS (NEIQSLV) are 1:0 (black), 1:0.4 (magenta), 1:3 (cyan), 1:5 (yellow), 1:10 (blue), 1:50 (red), 1:100 (green). (c) NMR titration curve for the titration of GIP with FAS (NEIQSLV). The plot shows the changes in the chemical shift of E67 induced by the addition of FAS (NEIQSLV), versus the peptide concentration. Dashed line is the titration curve as fitted by the program modelTitr from NMRPipe. The apparent dissociation constant K_D corresponding to residue E67 was determined by fitting the chemical shift change of the residue. The determined K_D value is 19.7 $\pm$ 2.1 μM.

derived from acrylamide quenching of soluble and refolded GIP are 14.5 M^{-1} and 14.4 M^{-1}, compared with 14.5 M^{-1} for *N*-acetyltryptophanamide (*47*). Iodide quenching is less efficient than that of acrylamide: the K_{sv} values for soluble and refolded GIP are 5.6 M^{-1} and 5.7 M^{-1} compared to 12.0 M^{-1} for *N*-acetyltryptophanamide (*47*). This decrease in K_{sv} value generated by iodide quenching of the fluorophore may be due to negatively charged neighboring residues at the operating pH of 6.5.

Fluorescence studies for all three ligands show consistent quenching of intrinsic tryptophan fluorescence intensity upon binding, which is indicative of a change in the environment of the fluorophore. The binding of the ligand to the protein may directly affect the fluorescence of a tryptophan residue with the ligand acting as a quencher, or by physically interacting with the fluorophore and thereby changing the polarity of its environment and/or its accessibility to solvent. Alternatively, the ligand may bind at a site on protein remote

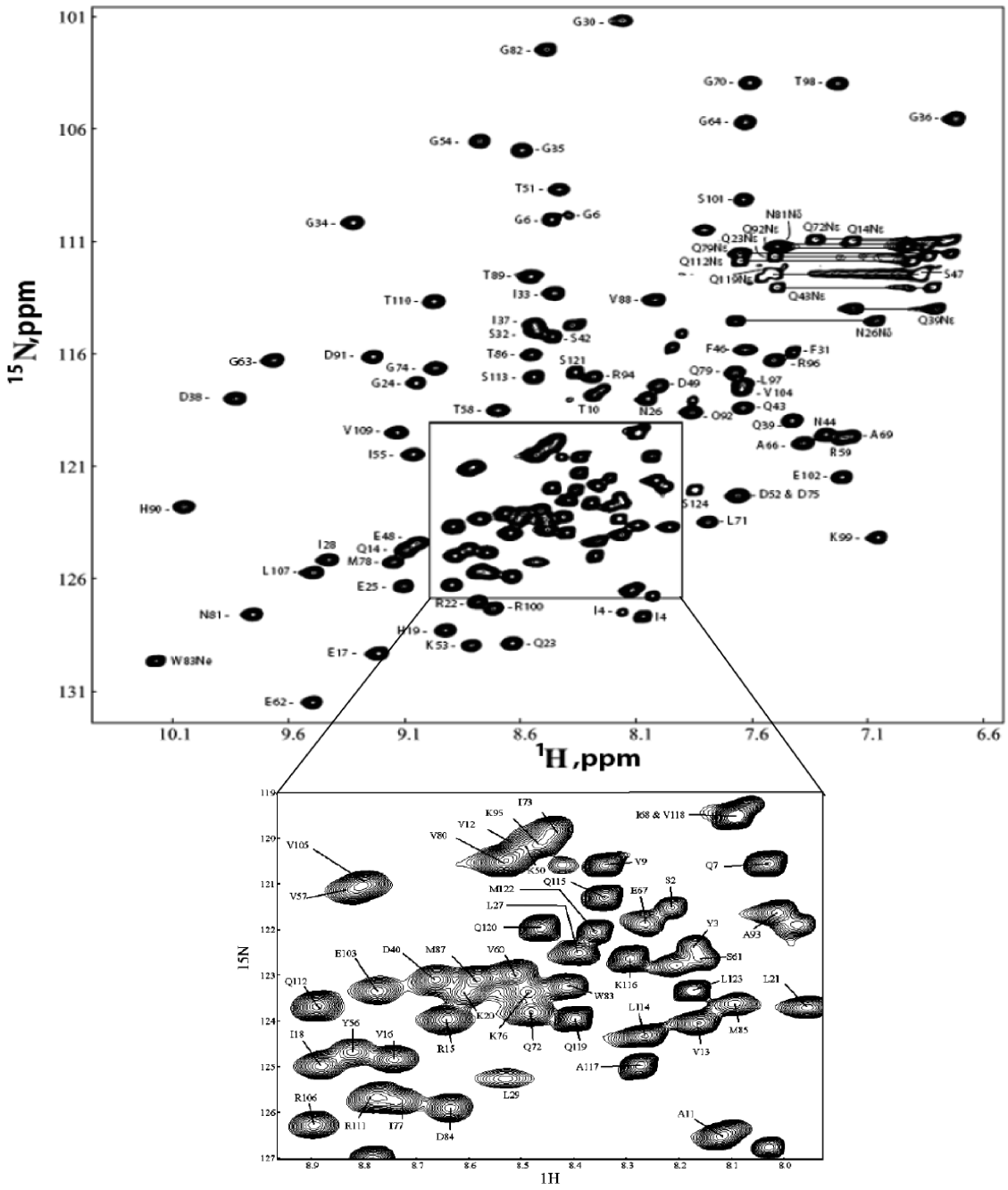

FIGURE 6: 2D {^{1}H,^{15}N }-HSQC spectrum of GIP at pH 6.2 and 25 °C. The assignment of the GIP is labeled in the HSQC spectrum.

from the tryptophan residue but can induce a protein conformational change, altering the microenvironment of the tryptophan (*48*). From our data, it could be concluded that the solvent exposed tryptophan of GIP was not directly involved in ligand binding; rather the ligands induced a conformational change of the GIP and thus altered the microenvironment of the tryptophan. The dissociation constants determined from the fluorescence intensity measurements revealed that the three ligands bind to GIP with similar affinities in the range of 1−10 μM. These moderate affinities are probably suitable for regulatory functions (*49*).

Deconvolution of CD data show that the amount of helix and random coil content in GIP decreases with increasing concentration of ligand while the amount of β-sheet increases. Thus the qualitative CD structural analysis is in excellent agreement with 2D HSQC titration data, which show chemical shift perturbation of GIP upon ligand binding.

It is worth noting that, from our NMR backbone assignment, Pro5 shows *cis*−*trans* isomerism, which results in multiple peaks of different intensities for its immediate neighboring residues, Ile4 and Gly6. Pro5 may play a key role in neurotransmitter-gated ion channel regulation by its *cis*−*trans* isomerism (*50*), and it may be associated with the neurotransmitter glutamate in the control of the ion channels in the synaptic junctions.

The secondary structure calculations from PSSI and PsiCSI show that the structure of GIP comprises 6 β-strands (β1−β6) and 2 α helices (α1 and α2) (Figure 7). The three-dimensional model of GIP (Figure 2) shows that the major part of the protein consists of a five-strand antiparallel β-sandwich formed by a three-strand β-sheet (β4, β5 and β6) and a two-strand β-sheet (β2 and β3). In the three-dimensional model, α2 orients parallel to β2, thus forming a groove, where the ligands for PDZ domain bind. The

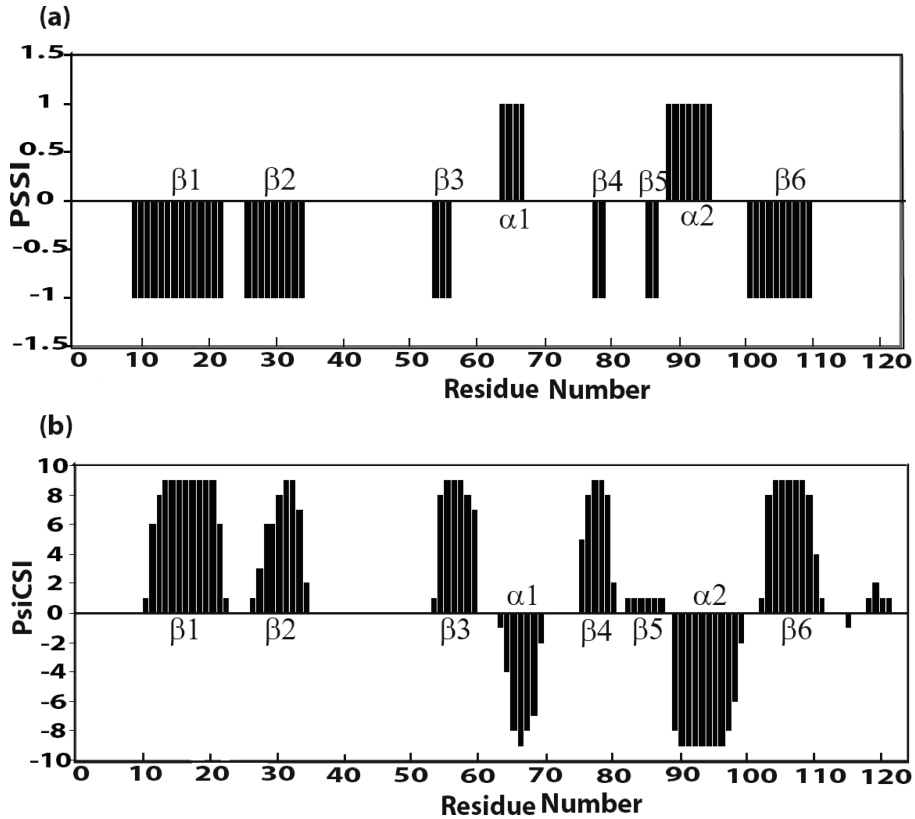

FIGURE 7: Consensus (using H_α, C_α and CO chemical shifts) chemical shift index (CSI) showing secondary structural elements of GIP using (a) PSSI and (b) PsiCSI programs.

mapping of ligand-induced chemical shift perturbations clearly indicates that the ligands bind to the canonical binding pocket, the β2 and α2 groove of GIP.

One important difference between the PDZ domain of GIP and other known PDZ domains is the substitution of the first glycine in the carboxylate-binding motif **G**LGF by Ile. The GLGF motif is highly conserved among PDZ domain. The second glycine in the GL**G**F motif is absolutely conserved, but a serine, threonine, or proline replaces the first glycine in a minority of PDZ domains (*3*). The exception to the GLGF motif is the PDZ domain of PDZ2 from human phosphatase hPTP1E with the SLGF motif (*51*). The strict requirement of a C-terminal free carboxyl group of the target protein for binding to PDZ domain is confirmed by the observation that C-terminal protected β-catenin (FDTDL-$CONH_2$) does not bind to GIP, since there is no change in the 2D HSQC titration data (data not shown). According to the peptide binding mechanism of class I PDZ domain (*52*), His90 in the α2 helix should contribute significantly to the binding of ligands C-termini i.e. the N-3 nitrogen of His residue might be forming a specific hydrogen bond with the hydroxylated side chains of either a serine or threonine residue, thus probably giving rise to preference for a particular residue at the P_{-2} position of class I PDZ domains. In fact, our HSQC titration results confirm that the chemical shift of His90 is affected greatly by the binding to C-termini recognition motifs of the target proteins.

It is clear from our HSQC titration data that chemical shifts for many of the amide signals of GIP change upon complex formation, which suggests that a significant conformational change in GIP might be occurring upon binding of ligands. How does the PDZ domain of GIP recognize different target sequences? What is the mode of interaction and recognition of these targets by the PDZ domain of GIP? A detailed structure−function investigation is needed to answer these questions.

CONCLUSIONS

The studies performed in this work represent important steps toward understanding the structure, and mode of interactions of a PDZ domain-containing multifunctional human protein. Results presented here also indicate that GIP undergoes a conformational change upon binding to ligand peptides. The 3D structure determination of GIP by high-resolution solution NMR is in progress. Structure, function, and interaction studies of GIP with different binding partners are critical to provide the insight into the mechanisms and role of this PDZ domain containing human protein in recognition, signaling and tumorigenesis, which indeed is a necessary prelude for successful drug design. Indeed, all the signal transduction pathways involving GIP can lead to cancer when unregulated. In fact, GIP regulates many of these signaling processes through its PDZ domain. To get an insight into cellular signaling, it is critical that we understand protein−protein interactions and how these communications regulate the well-being of a cell. Understanding the mechanisms of protein−protein interaction is a key step in addition to mapping out the signaling networks that engage PDZ domains.

ACKNOWLEDGMENT

We are grateful to Professor T. R. Webb and Ms. Uma Katre of Auburn University for critical reading of the

manuscript. We thank Ms. Amada R. Lopez de la Oliva (J. M. Laboratory) for GST-glutaminase bound resin and anti-GIP antibody and Dr. J. C. Aledo for help with GIP construct.

SUPPORTING INFORMATION AVAILABLE

Table S1, Optimization of the refolding of the GIP inclusion bodies; Table S2, Dissociation constants of various residues of GIP upon binding of different ligands by NMR; Figure S1, Fluorescence data of titration of GIP with peptides; Figure S2, CD data of titration of GIP with peptides, and Figure S3, Chemical shift perturbations of the GIP backbone amide groups upon binding with peptides. This material is available free of charge via the Internet at http://pubs.acs.org.

REFERENCES

1. Ponting, C. P., and Phillips, C. (1995) DHR domains in syntrophins neuronal NO synthases and other intracellular proteins. *Trends Biochem. Sci. 20*, 102–103.
2. Kennedy, M. B. (1995) Origin of PDZ (DHR, GLGF) domains. *Trends Biochem. Sci. 20*, 350.
3. Sheng, M., and Sala, C. (2001) PDZ domains and the organization of supramolecular complexes. *Annu. Rev. Neurosci. 24*, 1–29.
4. Hillier, B. J., Christopherson, K. S., Prehoda, K. E., Bredt, D. S., and Lim, W. A. (1999) Unexpected Modes of PDZ Domain Scaffolding Revealed by Structure of nNOS-Syntrophin Complex. *Science 284*, 812–815.
5. Bhat, M. A., Lzaddost, S., Lu, Y., Cho, K-O., Choi, K-W., and Bellen, H. J. (1999) Discs Lost, a Novel Multi-PDZ Domain Protein, Establishes and Maintains Epithelial Polarity. *Cell 96*, 833–345.
6. Kornau, H. C., Schenker, L. T., Kennedy, M. B., and Seeburg, P. H. (1995) Domain interaction between NMDA receptor subunits and the postsynaptic density protein PSD-95. *Science 269*, 1737–1740.
7. Kim, E., Niethammer, M., Rothschild, A., Jan, Y. N., and Sheng, M. (1995) Clustering of Shaker-type K+ channels by interaction with a family of membrane-associated guanylate kinases. *Nature 378*, 85–88.
8. Olalla, L., Aledo, J. C., Bannenberg, G., and Marquez, J. (2001) The C-terminus of human glutaminase L mediates association with PDZ domain-containing proteins. *FEBS Lett. 488*, 116–122.
9. Lobo, C., Ruiz-Bellido, M. A., Aledo, J. C., Márquez, J., and, NúñeZ De Castro, I., and Alonso, F. J. (2000) Inhibition of glutaminase expression by antisense mRNA decreases growth and tumourigenicity of tumour cells. *Biochem. J. 348*, 257–261.
10. Rousset, R., Fabre, S., Desbois, C., Bantignies, F., and Jalinot, P. (1998) The C-terminus of the HTLV-1 Tax oncoprotein mediates interaction with the PDZ domain of cellular proteins. *Oncogene 16*, 643–654.
11. Olalla, L., Gutiérrez, A., Jiménez, A. J., López-Téllez, J. F., Khan, Z. U., Pérez, J., Alonso, F. J., de la Rosa, V., Campos-Sandoval, J. A., Segura, J. A., Aledo, J. C., and Márquez, J. (2008) Expression of the scaffolding PDZ protein glutaminase-interacting protein in mammalian brain. *J. Neurosci. Res. 86*, 281–292.
12. Márquez, J., Lp̈ez, de la Oliva, A. R., Matés, J. M., Segura, J. A., and Alonso, F. J. (2006) Glutaminase: A multifaceted protein not only involved in generating glutamate. *Neurochem. Int. 48*, 465–471.
13. Hampson, L., Li, C., Oliver, A. W., Kitchener, H. C., and Hampson, I. N. (2004) The PDZ protein Tip-1 is a gain of function target of the HPV16 E6 oncoprotein. *Int. J. Oncol. 25*, 1249–1256.
14. Reynaud, C., Fabre, S., and Jalinot, P. (2000) The PDZ Protein TIP-1 Interacts with the Rho Effector Rhotekin and Is Involved in Rho Signaling to the Serum Response Element. *J. Biol. Chem. 275*, 33962–33968.
15. Alewine, C., Olsen, O., Wade, J. B., and Welling, P. A. (2006) TIP-1 Has PDZ Scaffold Antagonist Activity. *Mol. Biol. Cell 17*, 4200–4211.
16. Kanamori, M., Sandy, P., Marzinotto, S., Benetti, R., Kai, C., Hayashizaki, Y., Schneider, C., and Suzuki, H. (2003) The PDZ Protein Tax-interacting Protein-1 Inhibits β-Catenin Transcriptional Activity and Growth of Colorectal Cancer Cells. *J. Biol. Chem. 278*, 38758–3876.
17. Huber, A. H., Nelson, W. J., and Weis, W. I. (1997) Three-Dimensional Structure of the Armadillo Repeat Region of β-Catenin. *Cell 90*, 871–882.
18. Shibata, T., Chuma, M., Kokubu, A., Sakamoto, M., and Hirohashi, S. (2003) EBP50, a β-Catenin-Associating Protein, Enhances Wnt Signaling and Is Over-expressed in Hepatocellular Carcinoma. *Hepatology 38*, 178–186.
19. Itoh, N., and Nagata, S. (1993) A Novel Protein Domain Required for Apoptosis. *J. Biol. Chem. 268*, 10932–10937.
20. Saras, J., Engström, U., Góñez, L. J., and Heldin, C- H. (1997) Characterization of the Interactions between PDZ Domains of the Protein-tyrosine Phosphatase PTPL1 and the Carboxyl-terminal Tail of Fas. *J. Biol. Chem. 272*, 20979–20981.
21. Nagata, S. (1997) Apoptosis by Death Factor. *Cell 88*, 355–365.
22. Zhang, Q., Fan, J-S., and Zhang, M. (2001) Interdomain Chaperoning between PSD-95, Dlg, and Zo-1 (PDZ) Domains of Glutamate Receptor-interacting Proteins. *J. Biol. Chem. 276*, 43216–43220.
23. Aledo, J. C., Rosado, A., Olalla, L., Campos, J. A., and Marquez, J. (2001) Overexpression, Purification, and Characterization of Glutaminase-Interacting Protein, a PDZ-Domain Protein from Human Brain. *Protein. Expr. Purif. 23*, 411–418.
24. Delaglio, F., Grzesiek, S., Vuister, G. W., Zhu, G., Pfeifer, J., and Bax, A. (1995) NMRPipe: A multifunctional spectral processing system based on UNIX pipes. *J. Biomol. NMR 6*, 277–293.
25. Johnson, B. A., and Blevins, R. A. (1994) NMRView: A computer program for the visualization and analysis of NMR data. *J. Biomol. NMR 4*, 603–614.
26. Wang, Y., and Jardetzky, O. (2002) Probability-based protein secondary structure identification using combined NMR chemical-shift data. *Protein Sci. 11*, 852–861.
27. Hung, L. H., and Samudrala, R. (2003) PROTINFO: secondary and tertiary protein structure prediction. *Nucleic Acids Res. 31*, 3296–3299.
28. Hung, L. H., and Samudrala, R. (2003) Accurate and automated classification of protein secondary structure with PsiCSI. *Protein Sci. 12*, 288–295.
29. Coudevylle, N., Antoine, M., Bouguet-Bonnet, S., Mutzenhardt, P., Boschi-Muller, S., Branlant, G., and Cung, M-T. (2007) Solution Structure and Backbone Dynamics of the Reduced Form and an Oxidized Form of E. coli Methionine Sulfoxide Reductase A (MsrA): Structural Insight of the MsrA Catalytic Cycle. *J. Mol. Biol. 366*, 193–206.
30. Williamson, R. A., Carr, M. D., Frenkiel, T. A., Feeney, J., and freedman, R. B. (1997) Mapping the binding site for matrix metalloproteinase on the N-terminal domain of the tissue inhibitor of metalloproteinase-2 by NMR chemical shift perturbation. *Biochemistry 36*, 13882–13889.
31. Johnson, P. E., Tomme, P., Joshi, M. D., and McIntosh, L. P. (1996) Interaction of soluble cellooligosaccharides with the N-Terminal cellulose-Binding Domain of *Cellulomonas fimi* CenC. 2. NMR and Ultraviolet Absorption Spectroscopy. *Biochemistry 35*, 13895–13906.
32. Chipman, D. M., Grisaro, V., and Sharon, N. (1967) The binding of oligosaccharides containing *N*-acetylglucosamine and *N*-acetylmuramic acid to lysozyme. *J. Biol. Chem. 242*, 4388–4394.
33. Sreerama, N., and Woody, R. W. (2000) Estimation of Protein Secondary Structure from Circular Dichroism Spectra: Comparison of CONTIN, SELCON, and CDSSTR Methods with an Expanded Reference Set. *Anal. Biochem. 39*, 252–260.
34. Mao, H., Hajduk, P. J., Craig, R., Bell, R., Borre, T., and Fesik, S. W. (2001) Rational Design of Diflunisal Analogues with Reduced Affinity for Human Serum Albumin. *J. Am. Chem. Soc. 123*, 10429–10435.
35. Hu, H-Y., Horton, J. K., Gryk, M. R., Prasad, R., Naron, J. M., Sun, D-A., Hecht, S. M., Wilson, S. H., and Mullen, G. P. (2004) Identification of Small Molecule Synthetic Inhibitors of DNA Polymerase β by NMR Chemical Shift Mapping. *J. Biol. Chem. 279*, 39736–39744.
36. Harris, B. Z., and Lim, W. A. (2001) Mechanism and role of PDZ domains in signaling complex assembly. *J. Cell Sci. 114*, 3219–3231.
37. Jemth, P., and Gianni, S. (2007) PDZ domains: Folding and Binding. *Biochemistry 46*, 8701–8708.
38. Cavanagh, J. F., Wayne, J., Palmer, A. G., III, and Skelton, N. J. (1996) *Protein NMR Spectroscopy: Principles and practice*, Academic Press, Inc., San Diego, CA.

39. Schwede, T., Kopp, J., Guex, N., and Peitsch, M. C. (2003) SWISS-MODEL: an automated protein homology-modeling server. *Nucleic Acids Res. 31*, 3381–3385.
40. Guex, N., and Peitsch, M. C. (1997) SWISS_MODEL and the Swiss-PdbViewer: an environment for comparative protein modeling. *Electrophoresis 18*, 2714–2723.
41. Lindahl, E., Hess, B., and van der Spoel, D. (2001) GROMACS 3.0: a package for molecular simulation and trajectory analysis. *J. Mol. Model. 7*, 306–317.
42. Koradi, R., Billeter, M., and Wuthrich, K. (1996) MOLMOL: a program for display and analysis of macromolecular structures. *J. Mol. Graphics 14*, 51–55.
43. Gunther, J., Bergner, A., Hendlich, M., and Klebe, G. (2003) Utilising Structural Knowledge in Drug Design Strategies: Applications using Relibase. *J. Mol. Biol. 326*, 621–636.
44. Alston, R. W., Urbanikova, L., Sevcik, J., Lasagna, M., Reinhart, G. D., Scholtz, J. M., and Pace, C. N. (2004) Contribution of Single Tryptophan Residues to the Fluorescence and Stability of Ribonuclease Sa. *Biophys. J. 87*, 4036–4047.
45. Lehrer, S. S. (1971) Solute Perturbation of Protein Fluorescence. The Quenching of the Tryptophyl Fluorescence of Model Compounds and of Lysozyme by Iodide Ion. *Biochemistry 10*, 3254–3263.
46. Eftink, M. R., and Ghiron, C. A. (1976) Exposure of Tryptophanyl Residues in Proteins. Quantitative Determination by Fluorescence Quenching Studies. *Biochemistry 15*, 672–680.
47. McIntyre, J. C., Hundley, P., and Behnke, W. D. (1987) The role of aromatic side chain residues in micelle binding by pancreatic colipase. *Biochem. J. 245*, 821–829.
48. Ladokhin, A. S. (2000) in *Encyclopedia of Analytical Chemistry: Fluorescence Spectroscopy in Peptide and Protein Analysis* (Meyers, R. A., Ed.) pp 5762−5779, John Wiley & Sons, Chichester.
49. Nguyen, J. T., Turck, C. W., Cohen, F. E., Zuckerman, R. N., and Lim, W. A. (1998) Exploring the basis of proline recognition by SH3 and WW domains: design of N-substituted inhibitors. *Science 282*, 2088–2092.
50. Lummis, S. C., Beene, D. L., Lee, L. W., Lester, H. A., Broadhurst, R. W., and Dougherty, D. A. (2005) Cis-trans isomerization at a proline opens the pore of a neurotransmitter-gated ion channel. *Nature 438*, 248–252.
51. Kozlov, G., and Gehring, K. (2000) Solution Structure of the PDZ2 Domain from Human Phosphatase hPTP1E and Its Interaction with C-Terminal Peptides from the Fas Receptor. *Biochemistry 39*, 2572–2580.
52. Tochio, H., Zhang, Q., Mandal, P., Li, M., and Zhang, M. (1999) Solution structure of the extended neuronal nitric oxide synthase PDZ domain complexed with an associated peptide. *Nat. Struct. Biol. 6*, 417–421.

BI800287V